Complex Lasers with Controllable Coherence

Hui Cao[1]*, Ronen Chriki[2], Stefan Bittner[1], Asher A. Friesem[2], Nir Davidson[2]*

[1] Department of Applied Physics, Yale University, New Haven, CT, 06520, USA

[2] Department of Physics of Complex Systems, Weizmann Institute of Science, Rehovot 7610001, Israel

* Corresponding authors: hui.cao@yale.edu, nir.davidson@weizmann.ac.il

Abstract

The invention of lasers 60 years ago is one of the greatest breakthroughs in modern optics. Throughout the years, lasers have enabled major scientific and technological advancements, and have been exploited in numerous applications due to their advantages such as high brightness and high coherence. However, the high spatial coherence of laser illumination is not always desirable, as it can cause adverse artifacts such as speckle noise in imaging applications. To reduce the spatial coherence of a laser, novel cavity geometries and alternative feedback mechanisms have been developed. By tailoring the spatial and spectral properties of cavity resonances, the number of lasing modes, the emission profiles and the coherence properties can be controlled. This technical review presents an overview of such unconventional, complex lasers, with a focus on their spatial coherence properties. Laser coherence control not only provides an efficient means for eliminating coherent artifacts, but also enables new applications.

1. Introduction

1.1. Conventional lasers and coherence properties

Lasers have been widely used in industry, medicine and other areas of contemporary life, because of their high brightness, high coherence, high efficiency and good spectral control. The essential elements of a laser are a material that amplifies light through stimulated emission (the gain medium) and a cavity that traps light in the gain medium to enable more efficient amplification[1]. The gain medium is pumped electrically, by a current source, or optically, by a flash lamp or another laser source.

Figure 1 shows a common Fabry-Pérot (FP) laser cavity, consisting of two mirrors that face each other on either side of the gain medium[1]. Light bouncing back and forth between the mirrors is amplified each time it passes through the gain medium. A portion of the light leaves the cavity through one of the mirrors that is partially transmitting, producing an output beam. The resonance condition in such a cavity defines the longitudinal and transverse quantum numbers for a mode, which are equal to the numbers of field nodes in the longitudinal (perpendicular to mirrors) and transverse (parallel to mirrors) directions. Typically, the distance between the mirrors is much larger than the lateral dimension of the mirrors, thus modes propagate predominantly in the longitudinal direction, making the longitudinal quantum number much larger than the transverse one.

The lasing threshold is the pump power at which light amplification compensates the loss due to cavity leakage and material absorption. The light leakage from the cavity is characterized by the quality (Q) factor, which is proportional to the photon lifetime in the cavity. In a FP cavity, the Q factor of a resonance is nearly independent of the longitudinal quantum number but decreases with the transverse one. Hence, the lower-order transverse modes have lower thresholds and lase first at lower pump power. They will saturate the optical gain, especially for a homogeneously broadened gain spectrum, and prevent the higher-order modes from lasing at higher pump powers.

A key property of laser emission is its high degree of coherence[2]. The first-order coherence describes correlations of electric field E in space and time[3]. The degree of coherence is given by

$$g^{(1)}(r_1, r_2, \tau) = \frac{|\langle E^*(r_1, t)E(r_2, t + \tau)\rangle|}{\langle E^*(r_1, t)E(r_1, t)\rangle^{1/2}\langle E^*(r_2, t + \tau)E(r_2, t + \tau)\rangle^{1/2}}$$

where $\langle ... \rangle$ denotes averaging over time t. Specifically, the temporal coherence $g^{(1)}(\tau)$ describes the correlation of fields at the same location ($r_1 = r_2$) but different time, while the spatial coherence describes the correlation of fields at the same time ($\tau = 0$) but different locations. The width of $g^{(1)}(\tau)$ gives the coherence time, which is inversely proportional to the spectral width of the laser emission. In a FP cavity, only a few transverse modes lase, thus the spatial coherence is high. Note that the spatial coherence is independent of the number of longitudinal modes with identical transverse structure that lase. One way of reducing the spatial coherence is to increase the number of transverse lasing modes. An alternative way is to break the separability into longitudinal and transverse modes so that all lasing modes have distinct emission profiles.
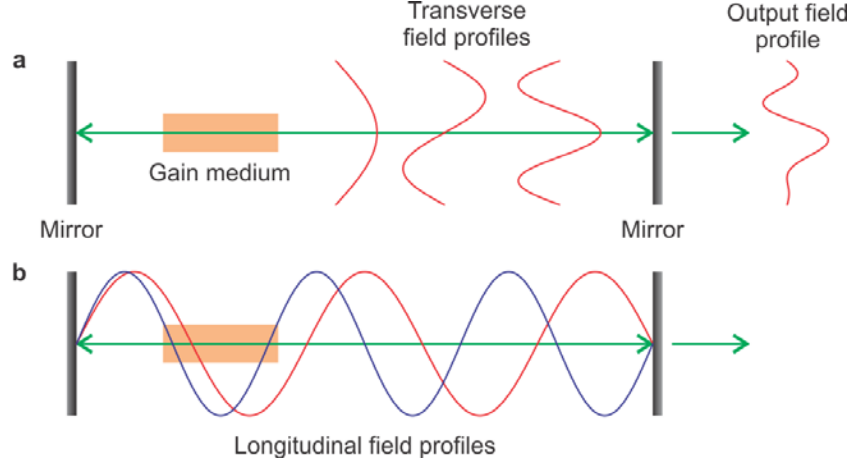
Figure 1: Schematic of a Fabry-Perot (FP) cavity laser. It consists of a pair of mirrors on either side of a gain medium. The cavity resonance condition determines **a** the transverse and **b** the longitudinal field profiles of the cavity modes.

High spatial and temporal coherences are not exclusive to lasers. Spatial or spectral filtering of spontaneous emission from a lamp can greatly improve spatial or temporal coherence. A fundamental difference between a laser and a lamp lies in the quantum statistical properties of their emission. On the time scale shorter than the characteristic time that is given by the inverse of the spectral bandwidth, laser light features Poissonian photon statistics, while the thermal light features Bose-Einstein statistics. More specifically, the statistical distribution of the photon number m in a single electromagnetic mode satisfies the Poisson distribution $P(m) = \langle m \rangle^m e^{-\langle m \rangle}/m!$ for laser light, and the Bose-Einstein distribution $P(m) = \langle m \rangle^m/[1 + \langle m \rangle]^{m+1}$ for thermal light, where $\langle m \rangle$ is the average photon number. The normalized second-order correlation coefficient, $g^{(2)} = \langle m^2 \rangle/\langle m \rangle^2$, quantifies the photon number fluctuations. In a laser, optical gain saturation suppresses intensity fluctuations of the emission, reducing the value of $g^{(2)}$ and enhancing the second-order coherence.

1.2. Coherent artifacts

A laser with high spatial coherence can generate a directional light beam with small divergence, and the beam can be focused to a diffraction limited spot. Unfortunately, high spatial coherence also causes deleterious effects such as coherent artifacts and cross-talk in full-field imaging and displays[4]. The most common manifestation of coherent artifacts is speckle noise[5]. A rough object or scattering environment introduces random phase delays among mutually coherent photons that interfere to produce a random grainy pattern[6]. In addition to parallel imaging and display applications, the coherent artifacts pose serious problems for laser applications in material processing, photolithography, holography, and optical trapping of cold atoms and colloidal particles.

To avoid coherent artifacts, incoherent sources such as lamps and light-emitting diodes (LEDs) are still used for most full-field imaging and display applications, in spite of having lower power per mode, poorer collection efficiency, and less spectral control than lasers. The power limitations are particularly problematical in imaging applications that involve absorbing or scattering media, prompting the use of raster-scanning modalities in laser-based imaging systems. However, scanning is time consuming and thus not suitable for imaging of moving objects or transient

processes. While parallel imaging can have high speed, it requires an illumination source with high power and low coherence.

Since speckle results from high spatial coherence, the most effective way of suppressing speckle is reducing the spatial coherence of a laser. The common approach resorts to techniques based on, e.g., spinning diffusers[7], colloidal solutions[8], or micro-electromechanical mirrors[9]. These techniques integrate over many uncorrelated speckle patterns in time, therefore requiring a relatively long integration time.

Another approach to suppress speckle is to exploit the low temporal coherence of broadband sources such as superluminescent diodes (SLDs) and supercontinuum sources. However, speckle suppression is less effective with low temporal coherence than with low spatial coherence, as illustrated in Fig. 2. Moreover, this approach cannot be adopted for applications that rely on narrowband lasers such as deep UV photolithography with excimer lasers.

Although various techniques have been developed over the years to reduce coherence artifacts, they are mostly applied outside the lasers themselves. Such approaches can be summarized as first making a laser with high spatial coherence, then reducing its coherence. An alternative approach, which would be more efficient, is to directly create a laser with low spatial coherence. Furthermore, the ability of tuning the spatial coherence of a laser will enable new applications as described below.
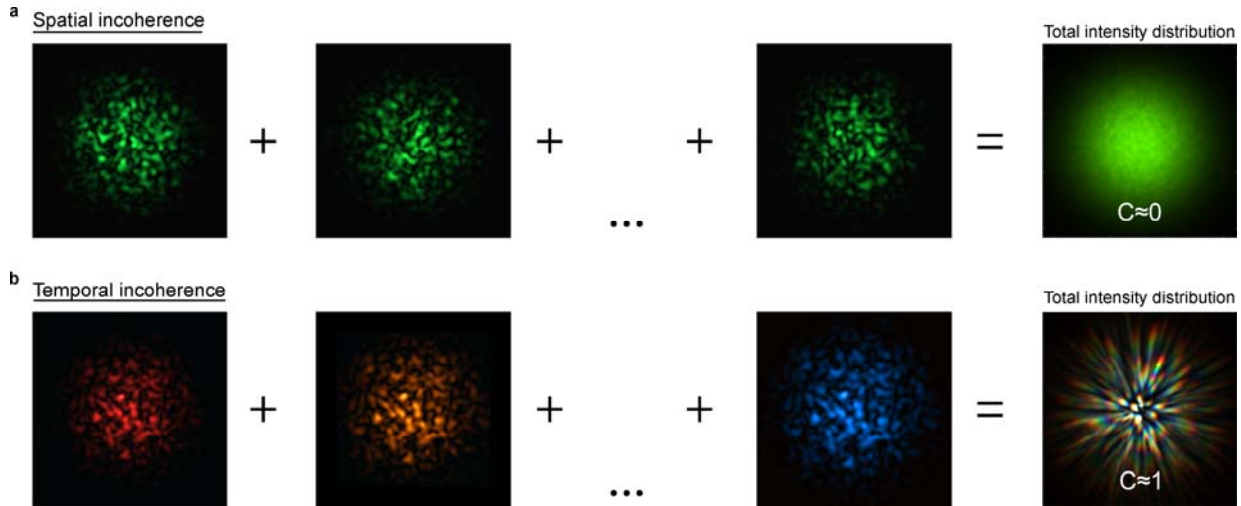

Figure 2: Speckle suppression with low spatial coherence or low temporal coherence. **a**, Low spatial coherence: light in different spatial modes is mutually incoherent. Each mode generates a distinct speckle pattern. The intensity sum of these speckle patterns reduces the contrast. **b**, Low temporal coherence: broadband light in a single spatial mode. Each wavelength generates an only marginally different speckle pattern: the wavelength difference results only in a radial rescaling of the generated speckle pattern, leading to a limited reduction of speckle contrast. Figure adapted from Ref.[10].

2. Lasers with low or tunable spatial coherence

2.1. Random lasers

Unlike conventional lasers that utilize mirrors or periodic structures to trap light, a random laser relies on light scattering in a disordered gain medium for optical feedback and confinement[11-13]. It has been implemented in various material systems, including powders[14], polycrystalline films[15], colloids[16], polymers[17], optical fibers[18] and organic materials[19]. The lasing frequencies range from ultraviolet[20] and visible[21] to infrared[22] and terahertz[23].

In a gain medium that consists of numerous scattering centers (Fig. 3a), the spontaneously emitted photons will be scattered many times and undergo a 'random walk'. Multiple scattering increases the path length of photons in the gain medium, thus enhancing the stimulated emission of photons that amplifies light[26,27]. Furthermore, the scattered waves may return to spatial positions they have visited before, providing feedback for lasing oscillation[28-30]. Experimentally, random lasing has been realized with both strong and weak scattering systems. The weaker the scattering, the higher the lasing threshold[31].

Most random lasers operate in the highly multimode regime. Individual lasing modes, formed by interference of scattered waves, have distinct frequencies and spatial structures[32,33]. The spatial distribution of field intensity for a lasing mode in a 2D diffusive medium[24] is plotted in Fig. 3b. When a large number of modes lase simultaneously with uncorrelated phases, their distinctly
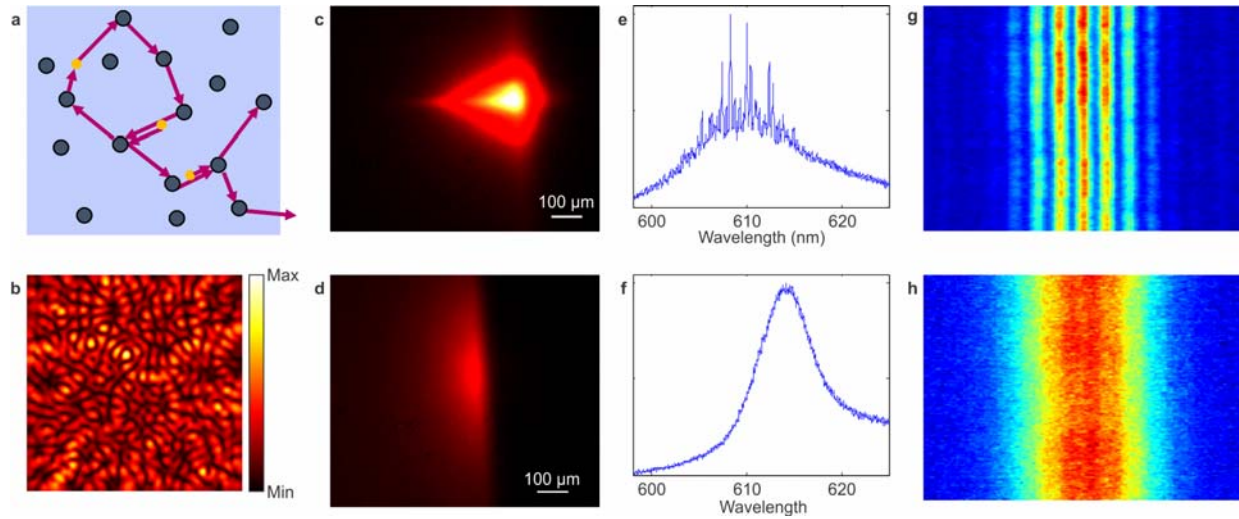

Figure 3: Spatial coherence of random lasers. **a**, Schematic of multiple scattering and stimulated emission of photons in a random medium. The black circles denote scattering centers, and the orange dots are excited atoms. **b**, Calculated spatial intensity distribution of a lasing mode in a 2D disordered structure. **c-h**, Experimental data for random lasers (colloidal solution with dye molecules pumped optically) in the weak (**c,e,g**) and strong (**d,f,h**) scattering regimes. **c,d**, Side-view images of the excitation volume. **e,f**, Normalized emission spectra for a single pump pulse with twice the lasing threshold energy. **g,h**, Far-field patterns of random laser emission through a double slit. The interference fringes with high contrast in **g** indicate the random laser in the weak scattering regime has high spatial coherence, while the lack of interference fringes in **h** reveals that the random laser in the strong scattering regime has low spatial coherence. Panel **b** adapted from Ref.[24], panels **c-h** adapted from Ref.[25].

speckled wavefronts combine incoherently to produce emission with low spatial coherence[34]. In stark contrast to the previous schemes of reducing the spatial coherence of a conventional laser by summing uncorrelated speckle patterns created sequentially by a time-varying scattering system (such as a spinning diffuser), the scatterers can be directly added into the laser cavity to simultaneously generate many distinct speckle patterns, each from a different lasing mode, to lower the spatial coherence. Furthermore, the number of the random lasing modes and their characteristic are dictated by the scattering length of the random medium (Fig. 3c-h) as well as the size and shape of the excitation volume. Thus the spatial coherence of random lasers can be tuned continuously by varying the density of scatterers or the pump beam profile[25].

Like a conventional laser, the temporal coherence of a random laser is determined by the spectral bandwidth of the emission[35,36]. The photon statistics of a random laser is more complex than that of a conventional laser[37]. Well above the lasing threshold, gain saturation quenches the fluctuation of the total photon number in all lasing modes[38,39], but strong mode coupling can cause photon number fluctuations in individual modes[40-42]. In strong scattering systems, the coupling of lasing modes is reduced, and the photon number fluctuation in each mode can be quenched by gain saturation well above the threshold[43,44].

2.2. Chaotic microcavity lasers

While the ray dynamics in conventional laser cavities such as the FP cavity is regular, cavities with complex geometries can exhibit chaotic ray dynamics[45]. Nevertheless, the modes of the passive resonators are given by a linear wave equation, and hence cannot exhibit chaos in the sense of an exponential sensitivity to the initial conditions. Instead, the chaotic ray dynamics is manifested in the properties of the modes[46], leading to qualitatively different spectral properties and spatial mode structures compared to cavities with regular ray dynamics. For example, the modes have non-degenerate frequencies, and their field distributions typically have a pseudo-random, speckle-like structure in the case of chaotic ray dynamics[47]. Due to the non-separable geometry of chaotic cavities, the resonant modes can no longer be assigned longitudinal and transverse quantum numbers. Most studies on chaotic microcavity lasers concern the steady-state lasing properties such as output directionality, lasing threshold and emission spectrum[48].

Here we focus on the spatial coherence of chaotic microcavity lasers. Let us consider a two-dimensional (2D) circular cavity of radius R with a section removed along a straight cut at a distance r_0 from the center of the circle. The ray dynamics in such a cavity, also called "D-shaped cavity", is chaotic[49]. A D-shaped dielectric disk supports a large number of resonances with relatively high but similar quality (Q) factors, which can hence lase with almost identical threshold[50]. Because their spatial profiles are spread over the entire cavity, their competition for gain is reduced as compared to whispering gallery modes that are concentrated near the boundary of, e.g., a circular cavity (Fig. 4). Consequently, this cavity supports a large number of lasing modes. Optimizing the ratio r_0/R of the D-cavity can further reduce the difference in their lasing thresholds and minimize their competition for gain, thus maximizing the number of lasing modes. Experimentally it has been demonstrated that more than 1000 modes lase simultaneously and independently in a D-shaped GaAs microdisk[50]. This is in sharp contrast to a circular microdisk in which only a small number of extremely high-Q whispering gallery modes lase. Unlike the longitudinal modes of a FP cavity, all lasing modes in a D-shaped cavity have distinct emission profiles and thus all contribute to the reduction of spatial coherence of the emission.
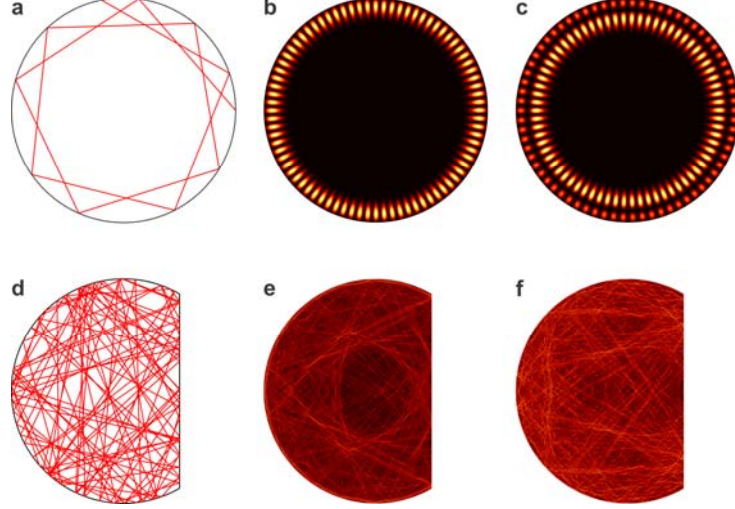
Figure 4: Resonant modes in 2D microcavities with regular or chaotic ray dynamics. **a**, Whispering gallery trajectory in a circular cavity staying close to the cavity boundary. **b, c**, Spatial intensity distributions of two whispering gallery modes in a circular dielectric disk that are confined to the disk boundary. **d**, A typical ray trajectory in a D-shaped cavity spreads over the entire cavity due to the chaotic ray dynamics. **e,f**, Spatial intensity distributions of two resonances in a D-shaped dielectric disk displaying a pseudo-random speckle-like structure.

2.3. Broad-area VCSELs and VCSEL arrays

Vertical-cavity surface-emitting lasers (VCSELs) have extremely short cavity lengths of the order of one wavelength, thus emitting in a single longitudinal mode[51]. For a small enough aperture diameter of a few micron, the VCSEL supports only the fundamental transverse mode with an output power up to 10 mW. To increase the power, broad-area VCSELs are developed, with aperture diameters up to 100 μm and CW output powers up to 100 mW. They operate with a multitude of higher-order transverse modes, resulting in spatially structured and more divergent far-field beam profiles[52-54]. The multi-transverse mode emission is accompanied by complex emission dynamics, which can be observed as a combination of spatio-temporal and polarization dynamics[55-57].

When a broad-area VCSEL is driven by a short current pulse, the interplay between a rapid thermal chirp and the formation of a spatially distributed thermal lens causes the break-up of the global cavity modes[58]. The system becomes so unstable that no lasing modes can build up. Instead the VCSEL operates in a non-modal state with very low spatial coherence. Namely, it lases in a superposition of independent "coherence islands" with dimensions of a few micrometers instead of in cavity modes[59]. The spatial decoherence manifests itself in the formation of a Gaussian far-field intensity distribution. By tuning the pump pulse duration and amplitude, the spatial coherence of these VCSELs can be varied[60]. This provides a simple way to generate partially coherent, highly directional beams[61], but it works only in the transient regime. An alternate device suitable for steady state operation is a 2D array of VCSELs. Since individual lasers are uncoupled and mutually incoherent, their combined emission has low spatial coherence[62].

2.4. Degenerate cavity laser

A large number of transverse lasing modes can be obtained with a degenerate cavity, in which all transverse modes have identical Q factors[64,65]. One example, shown in Fig. 5a, is a cavity comprised of two flat mirrors, in between which are two lenses in a 4f telescope arrangement. This constitutes a self-imaging system, which is a general property of all degenerate cavities. Namely, an arbitrary field distribution at any plane in the cavity is accurately imaged onto itself after one round trip. Therefore, any field distribution is an eigenmode of the cavity, and all (orthogonal) eigenmodes are degenerate. Since the lasing thresholds of the transverse modes are nearly identical, all transverse modes can lase simultaneously. The number of transverse lasing modes is given by the ratio of the gain medium cross-section over the diffraction limited area, which is determined by the smallest NA of the elements inside the cavity. Experimentally, more than 10^5
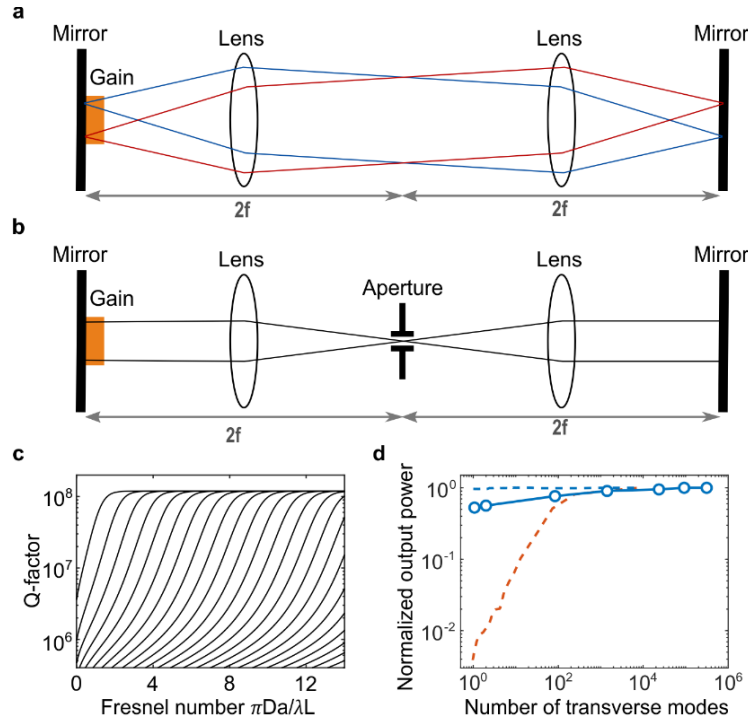
Figure 5: Degenerate cavity laser with tunable spatial coherence. **a**, Schematic of a degenerate laser cavity in the self-imaging configuration. Light emitted from any point in the gain medium will be imaged back to itself after one round trip. A large number of independent transverse modes lase simultaneously and independently to produce low spatial coherence. **b**, Inserting an aperture in the mutual focal plane of the two lenses yields a single transverse mode emitting with high spatial coherence. **c**, Cavity Q-factors as a function of the Fresnel number (proportional to the aperture diameter) for a 1 m long degenerate cavity with an output coupler of 90% reflectivity. As the aperture size increases, additional transverse modes appear and their Q factors rise quickly to approach the value of existing modes. **d**, Measured output power as a function of the number of transverse modes in the degenerate cavity (solid blue line), compared to calculated output power vs. number of modes for a degenerate cavity laser (blue dashed line) and a stable hemispherical cavity (red dashed line). Panels **a** and **b** adapted from Ref.[63].

transverse modes lasing simultaneously has been realized in a degenerate solid-state laser, resulting in emission with extremely low spatial coherence[66].

To tune the degree of spatial coherence, the number of transverse lasing modes can be varied by inserting a variable circular aperture in the mutual focal plane of the two lenses[66]. As shown in Fig. 5b, the aperture serves as a spatial filter that introduces loss to higher order transverse modes. When the aperture is sufficiently small, only the lowest-order transverse mode will lase. Since the spatial overlap of the lasing mode and the gain medium remains the same, the total power extracted from the gain medium is nearly unchanged. By decreasing the size of the aperture, the number of transverse lasing modes can be reduced from 320,000 to 1, while the output power decreases by less than 50%. The remarkable efficiency of redistributing energy over 10^5 transverse modes is unique for the degenerate cavity laser, and not possible with conventional laser resonators (Fig. 5d). Thanks to the self-imaging characteristic, the lasing modes can have arbitrary transverse profiles. Thus there is no inherent mode size, allowing the laser to adopt any mode size dictated by the aperture. For conventional laser resonators, however, the characteristic mode size is dictated by the cavity geometry, thus spatial filtering inevitably introduces loss in all modes due to the inherent mismatch. Traditionally, the spatial coherence of emission is tuned via spatial filtering outside the laser cavity, but then the total power reduces linearly with the number of transverse modes, assuming all modes have equal power. Hence, spatial filtering outside the laser results in much lower efficiency than filtering inside a degenerate cavity.

A further manipulation of the spatial coherence properties is obtained by resorting to more sophisticated intra-cavity spatial filters (masks) in the degenerate cavity laser[67]. For example, a variable slit which enables independent control of the spatial coherence length in one coordinate axis without affecting that in the other axis; two pinholes, an annular band and an array of circular holes can generate cosine, Bessel and comb-like spatial coherence functions, respectively. In principle, arbitrary spatial coherence functions can be obtained with a degenerate laser without losing power.

2.5. Multimode fiber amplifier

High-power fiber laser amplifiers have been replacing conventional solid-state laser amplifiers in many applications because of their compactness, robustness, and high efficiency[68,69]. While increasing the fiber core diameter allows scaling up the pulse energies and peak powers, it leads to a degradation of the output beam quality as multiple guided modes in a fiber compete for gain. The multimode nature of the fiber core can be mitigated by use of a mode-filtering effect in a coiled low-numerical-aperture fiber core, yielding a significant improvement in output-beam quality[70]. Alternatively, appropriate structuring of the seed beam wavefront can shape the light amplified by a multimode fiber[71]. Output beam narrowing and cleaning, as well as spatial and temporal focusing, are realized by adaptive control of the input wavefront[72].

Without an external seed, a fiber amplifier produces amplified spontaneous emission (ASE). The ASE has a broad spectrum and low temporal coherence. The spatial coherence of ASE depends on the number of fiber modes. A single-mode fiber produces ASE with high spatial coherence, while a multimode fiber can greatly reduce the spatial coherence. The recently developed optical fiber with an extra-large mode area (XLMA) gain core supports numerous guided modes and produces ASE with low spatial coherence[73]. The end facets of the fiber are cleaved at an angle to minimize feedback which could lead to lasing, similar to a semiconductor-based super-luminescent diode

(SLD). However, the ASE produced by a semiconductor SLD has relatively high spatial coherence, because it is based on one-dimensional waveguide that has a limited number of transverse modes[74]. The fiber is a waveguide with 2D cross section which supports many more guided modes. Furthermore, fiber bending and imperfections (fluctuations of the refractive index and variations of the fiber cross section) introduce random coupling among the modes, which tend to equalize the gain experienced by different modes. The reduction of mode-dependent gain in the multimode fiber favors highly multimode operation, leading to low spatial coherence. Therefore, a multimode-fiber-based ASE source combines low temporal coherence with low spatial coherence[73].

3. Applications of complex lasers

3.1. Speckle suppression

A fully developed speckle pattern satisfies Rayleigh statistics[75]. The intensity contrast $C = \sigma_I/\langle I \rangle$ is equal to 1, where σ_I is the standard deviation of the intensity and $\langle I \rangle$ is the average intensity. Summing the intensities of N uncorrelated speckle patterns reduces the contrast by a factor of $\sqrt{N}$. Experimentally, the observed speckle contrast depends on the exposure time of the detector. For example, let us consider a laser with N spatial modes, which are frequency degenerate. Each has a linewidth of $\delta\omega$, corresponding to a coherence time $\tau_c = 1/\delta\omega$. When illuminating a static scattering medium, each mode generates a distinct speckle pattern. If the exposure time is less than the coherence time, all modes are phase coherent with each other, and their scattered fields will add coherently to form a new speckle pattern with unity contrast. However, if the exposure time is much longer than the coherence time, the modes become mutually incoherent and their speckle patterns add in intensity, lowering the contrast to $1/\sqrt{N}$.

If the spatial modes are non-degenerate, their frequency difference will accelerate the dephasing. Assuming the frequency spacing of spatial modes $\Delta\omega$ exceeds their linewidth $\delta\omega$, they become mutually incoherent for an exposure time longer than $1/\Delta\omega$. Therefore, the spectral repulsion of lasing modes in a random medium[28] or a chaotic cavity[47] shortens the exposure time that is needed for speckle suppression.

In a degenerate cavity[10], the frequency spacing between the longitudinal modes $\Delta\omega_l$ is usually much larger than that of the transverse modes $\Delta\omega_t$. On the short time scale of $1/\Delta\omega_l$, the coupling between the longitudinal modes and the transverse modes reduces the speckle contrast to $1/\sqrt{M}$, assuming the number of longitudinal modes M is less than the number of transverse modes N. On the long time scale of $1/\Delta\omega_t$, the longitudinal modes no longer contribute to the speckle reduction, all transverse modes add incoherently and the speckle contrast becomes $1/\sqrt{N}$.

Typically, it is easier to manipulate the spatial coherence than the temporal coherence of a laser. The spatial coherence is determined by the number of spatial (transverse) lasing modes, which can be controlled by the cavity geometry and/or internal structure, while the temporal coherence is dictated by the emission bandwidth, which depends on the gain medium. Generally, the schemes for reducing the spatial coherence, as described in the previous section, are applicable to a variety of lasers that can operate at different wavelengths and with different gain materials. An alternative way of lowering the spatial coherence, which is applicable for a broadband source, is to transform temporal incoherence to spatial incoherence via spectral or spatial dispersion[76-78].

3.2. Speckle-free imaging

The ability of a laser with low spatial coherence to suppress speckle noise directly translates to improved image quality, especially when imaging in a scattering environment[79]. Figure 6 shows examples of full-field imaging through a static scattering film of an Air Force test chart with four illumination sources. Under spatially coherent illumination with a conventional narrowband laser, interference among these scattered photons results in speckle that corrupts the image beyond recognition. Even though a broadband laser or an ASE source has relatively low temporal coherence, the speckle noise is still too large to resolve the features of the object. In contrast, when illuminating with a random laser of low spatial coherence, interference between scattered photons is prevented, leading to a uniform background level. Although the scattered photons that are mis-
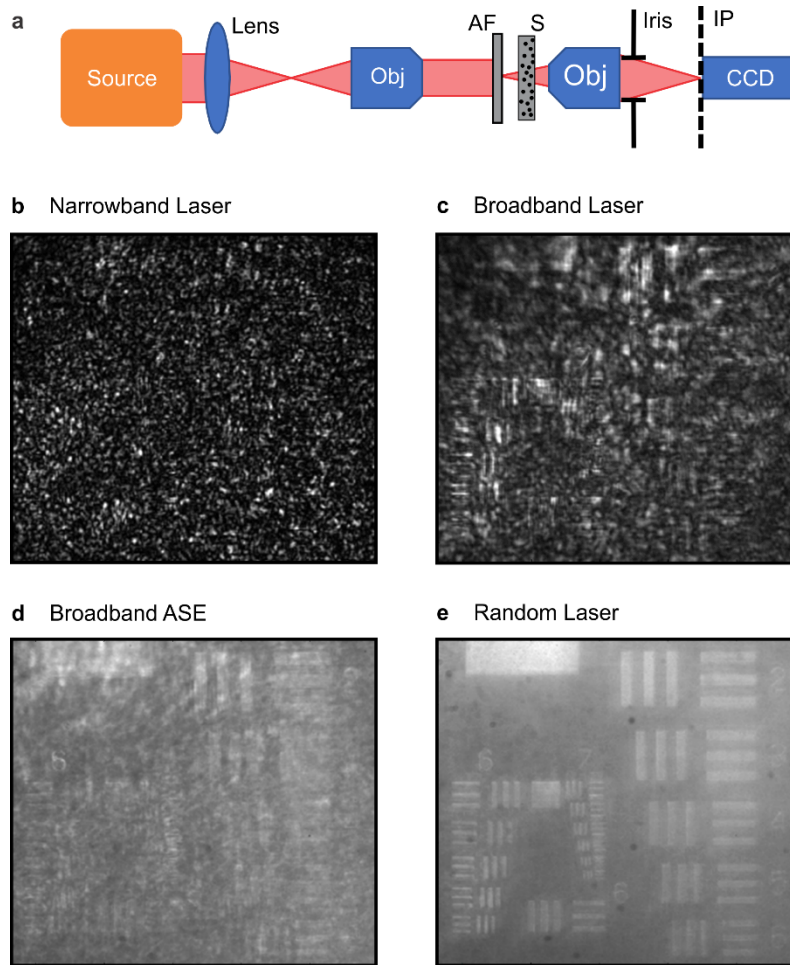

Figure 6: Speckle-free full-field imaging. **a**, Schematic of the experimental setup to image an Air Force resolution test chart (AF) through a thin static scattering film (S). The scattering film is placed between the test chart and the objective (Obj) which images the test chart on the CCD camera. **b-e**, Images taken with four different illumination sources, a narrowband laser (**b**), a broadband laser (**c**), an ASE source (**d**), and a random laser (**e**). The first three sources have high spatial coherence, resulting in significant speckle noise, and the last one has low spatial coherence, yielding a speckle-free image. Figure adapted from Ref.[79].

mapped to what would otherwise be dark regions of the image increase the background level and lower the image contrast, the features of the object remain clearly visible. It has been shown in another experiment that even a narrow-band random laser, which has high temporal coherence, can provide speckle-free illumination for full-field imaging[80].

The speckle noise depends not only on the coherence properties of the illumination source, but also on the imaging optics, including the ratio of the numerical aperture for observation to that for illumination[81]. Therefore, the degree of spatial incoherence of an illumination source that is needed to suppress speckle noise depends on the parameters of a specific application, such as the amount of scattering, the imaging resolution, etc. Consequently, a multimode laser can be designed to provide sufficiently low spatial coherence for speckle suppression, while maintaining relatively high power per mode as compared to existing spatially incoherent sources such as lamps and LEDs. For example, about 1000 spatial modes are enough to suppress speckle below the level observable by humans, but lamps and LEDs emit photons into far more modes, thus having lower brightness.

A quantitative measure of the source brightness is the photon degeneracy parameter δ, which gives the number of photons per coherence volume[2]. It is proportional to the spectral radiance, a radiometric measure of the amount of radiation through a unit area and into a unit solid angle within a unit frequency bandwidth. The values of δ for random lasers and chaotic microcavity lasers are several orders of magnitude higher than those of lamps and LEDs[50]. The greatly improved photon degeneracy allows much shorter exposure time and much higher speed for full-field imaging of transient processes. For example, a random laser can be triggered to produce a short illumination flash at a well-defined delay time, providing uniform, speckle-free background illumination[82]. It enables time-resolved microscopy with an exposure time as short as 10 ns.

3.3. Spatial coherence gating

Confocal microscopy combines high spatial resolution with improved contrast and optical sectioning[83]. Traditional confocal microscopes rely on raster scanning, which limits image acquisition speed[84]. The most common approach to parallelization is using an array of spatially separated pinholes[85]. These pinholes must be sufficiently separated to prevent cross talk. An alternative approach to completely parallelize confocal image acquisition is to combine interferometric detection with spatial coherence gating[86]. In this approach, each spatial mode (defined by the spatial coherence area) acts as a virtual pinhole, since interference only occurs for light from a single spatial mode. Unlike physical pinholes, these virtual pinholes do not require physical separation to avoid cross talk, enabling parallel acquisition of an entire *en face* plane in a single snapshot without scanning. Although this type of microscope cannot be used for fluorescence imaging, it has the potential for high-speed, large-area reflectance imaging with confocal resolution and sectioning. However, it requires a light source that not only has low spatial coherence but also has sufficient power per mode.

Fig. 7 shows an interferometric confocal microscope using an array of 1200 VCSELs coupled to a multimode fiber[87]. The interferometric detection, achieved with an off-axis holography technique, enables parallel acquisition of image information from 18,000 continuous virtual pinholes. The number of virtual pinholes is not limited to the number of emitters in the VCSEL array since these lasers are combined to eliminate cross talk through averaging, rather than as independent imaging channels. Instead, the number of virtual pinholes is limited by the number of resolvable elements provided by the microscope objective, which is determined by the field of view and the point spread function. The interferometric detection of low spatial coherence fields
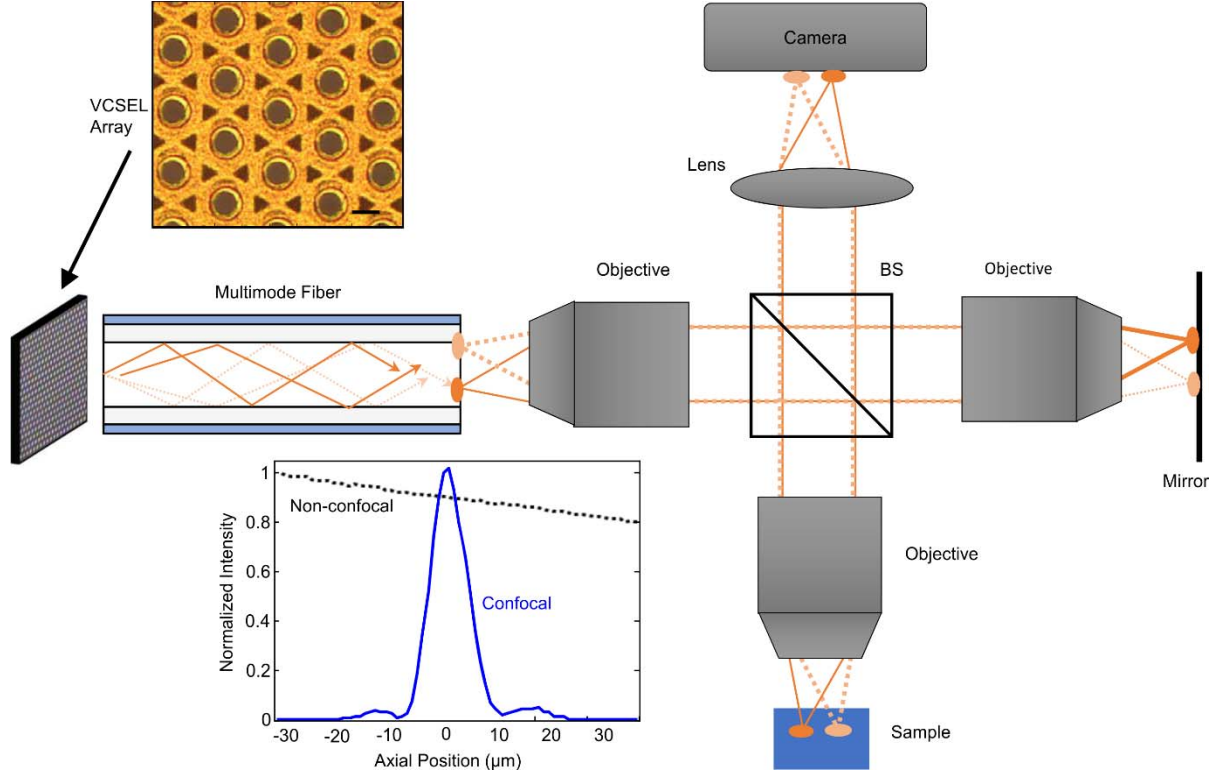
Figure 7: Full-field interferometric confocal microscope. The VCSEL array is coupled to a multimode fiber, which mixes mutually incoherent emission from 1200 independent lasers and provides a uniform low-spatial-coherence illumination on the sample. Light reflected from the sample combines with that from the mirror at the beam splitter (BS), and their interference patterns are recorded by the camera. The top left inset shows part of the VCSEL array where each circle of ~20 μm diameter represents an emitter. The bottom left inset shows the axial point spread function (blue solid line), whose width gives the axial resolution ~8 μm. The black dotted line represents the conventional wide-field microscope in which the recorded intensity decays slowly with defocus. Figure adapted from Ref.[87].

yields a coherent signal that is inherently confocal in the transverse plane and along the axial dimension. The microscope in Fig. 7 provides *en face* images with a 210 μm × 280 μm field of view, ~2 μm lateral resolution, and ~8 μm axial resolution in a single shot. The high photon degeneracy shortens the integration times to 100 μs, and increases the 2D frame rates to above 1 kHz. The interferometric detection also recovers the phase of the optical field, which can be used to estimate the height of sub-resolution axial features. The coherent noise from a highly scattering sample is strongly suppressed by the low spatial coherence illumination[88]. The ultrahigh-speed, full-field holographic confocal microscopy has been applied to *in vivo* quantitative studies of microscale physiology[89].

3.4. Bi-modal imaging

While a speckle-free wide-field image provides the structural information of an object, the speckle formed by random scattering of coherent light carries additional information about the motion of the object. For example, dynamic scatterers in a biological sample, such as moving blood cells, induce phase shifts in the scattered light, causing temporal changes in the speckle pattern. Such changes can be used to map the blood flow in living tissue by a technique called laser speckle contrast imaging[90].

To obtain both anatomical and functional information on living tissue, bimodal imaging is explored, e.g., to combine laser speckle contrast microscopy for mapping neural blood flow and an intrinsic signal optical imaging for monitoring tissue oxygenation. This is achieved by using two separate illumination sources, a laser and a LED, and switching rapidly between them[91]. However, a single illumination source with tunable spatial coherence but constant power would be desirable for such applications. While the spatial coherence of a LED could be increased by spatial filtering, the power would be greatly reduced. The best scenario is to tune the spatial coherence of a laser such as the degenerate cavity laser with little power loss[66,67]. An electrically-pumped semiconductor-based degenerate VECSEL (vertical external cavity surface emitting laser) with continuous wave (CW) emission was developed for imaging embryo heart function in a Xenopus, an important animal model of heart disease[63]. The low-spatial-coherence illumination is used for high-speed (100 frames per second) speckle-free imaging of the dynamic heart structure, and the high-spatial-coherence illumination for laser speckle contrast imaging of the blood flow.

3.5. Laser wavefront shaping

A degenerate laser supports a large number of transverse modes with almost identical frequencies but different spatial wavefronts. These modes can be superposed to produce arbitrary output beam profiles. This property is useful for beam shaping optics, which becomes a key technology for the applications of high power lasers to materials processing and device fabrications[92]. External reshaping of a laser beam (outside of the laser cavity) to a desired transverse profile has been implemented by a variety of methods including diffractive optical elements, free-form optics or digital holography with a spatial light modulator (SLM). For example, an aspheric or diffractive beam shaper transforms a Gaussian intensity profile of a single-mode laser beam to a flat-top beam. However, a multimode degenerate laser can directly generate an output beam with flat-top profile[93]. In fact, any beam profile can be produced by inserting an amplitude mask inside a degenerate cavity close to the output coupler or the end mirror.

Due to diffraction, the beam profile changes during propagation. By manipulating the spatial coherence, the variation of the beam profile with propagation distance can be controlled[94]. In the 4f degenerate cavity (Fig. 5), direct access to both the real space and the Fourier space of the lasing modes enables simultaneous control of the beam profile and the spatial coherence. Shaped beams with tailored spatial coherence can be obtained by applying an amplitude mask near one of the mirrors and a Fourier mask in the mutual focal plane of the two lenses[95]. If the Fourier mask is a circular aperture, decreasing the aperture diameter removes the components with a large transverse wave vector. The output beam experiences less diffraction upon propagation, but the minimal feature size of its spatial profile is increased. To produce a shaped beam that is propagation invariant, the Fourier mask should be an annual aperture (see Fig. 8a) so the spatial coherence function of the emission becomes a Bessel function. The output beam, regardless of its transverse profile (which is set by an amplitude mask inside the degenerate cavity), can propagate over a long
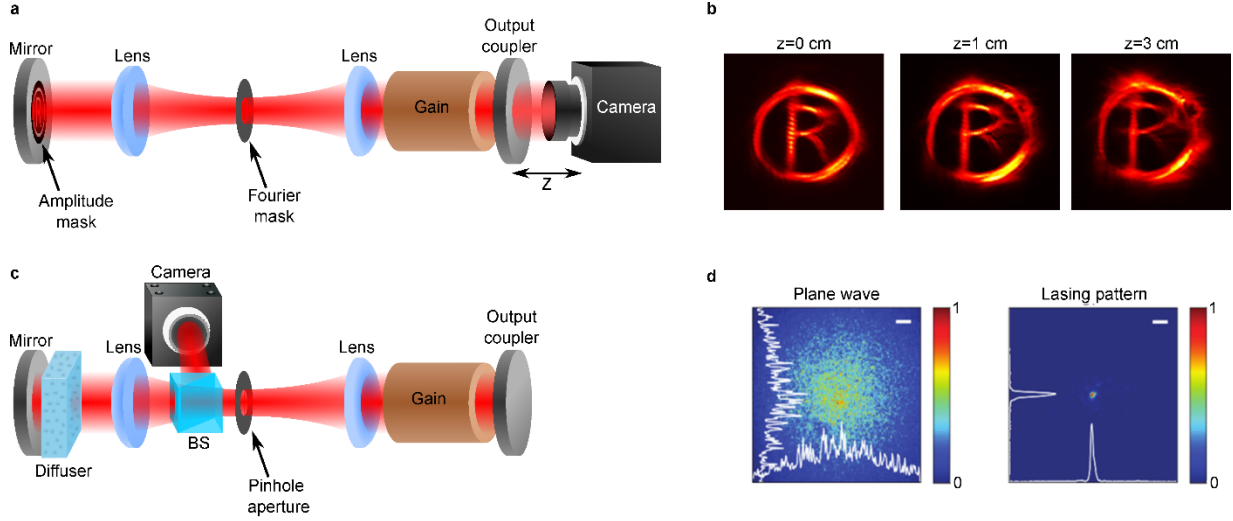
Figure 8: **a,b**, Generation of propagation-invariant beams in a degenerate laser cavity. **a**, An amplitude mask is placed close to the back mirror, and an annular ring in the mutual focal plane of the two lenses. **b**, The resulting output beam maintains its transverse profile for relatively long propagation distances. **c,d**, Focusing light through a scattering medium. **c**, An optical diffuser is placed inside the degenerate cavity near the output coupler, while a small pinhole aperture is placed at the Fourier plane for focusing of laser light. **d**, Intensity distribution at the plane of the pinhole aperture (right panel), recorded by the camera with a beam splitter (BS), compared to focusing of light through a scattering medium (outside the cavity) by wavefront shaping with a spatial light modulator (left panel). Panel **a** adapted from Ref.[95], panel **d** adapted from Ref.[96].

distance with minimal diffraction, as shown in Fig. 8b. Furthermore, multi-tasking geometric phase metasurfaces can be incorporated into a modified degenerate cavity laser as an output coupler to efficiently generate spin-dependent twisted light beams of different topologies[97].

In addition to shaping the output beam, the intracavity wavefront of the laser light can be tailored for penetrating through a random scattering medium, which is placed inside a degenerate cavity[96]. Focusing of light scattered by a rapidly varying disordered sample at sub-microsecond timescales has been realized without requiring a computer-controlled SLM or electronic feedback. As shown in Fig. 8c, by inserting a pinhole in the mutual focal plane of the two lenses in the degenerate cavity, the lasing state finds a complex wavefront that focuses the maximum power to the pinhole in order to minimize the loss. This approach relies on the self-organization of the optical field inside the degenerate cavity to create an optimal wavefront that forms a sharp focus from the otherwise randomly scattered light. This wavefront effectively compensates the effect of scattering induced by the random medium. Such wavefront shaping is achieved by all optical feedback, and is therefore orders of magnitude faster than all other wavefront shaping techniques.

4. Conclusions and outlook

In contrast to traditional laser resonators with relatively simple configurations, the lasers covered in this technical review employ complex structures and geometries. In spite of their differences, these unconventional lasers all possess a large number of spatial degrees of freedom. Thus they can display rich behaviors and novel properties that are absent for conventional lasers. By tailoring

the spatial structures of lasing modes, nonlinear modal interactions via the gain material can be controlled. Consequently, the number of lasing modes and the spatial coherence of emission can be tuned over a wide range. Furthermore, the output beams can have arbitrary profile and topology. These complex lasers enable new applications, such as high-speed speckle-free imaging, spatial coherence gating and focusing through scattering media. The different types of lasers reviewed here each have unique properties and are suitable for various applications with specific demands.

Complex lasers also have additional advantages over traditional lasers. The wave-chaotic micro-cavity lasers, as well as the random lasers, can suppress spatio-temporal instabilities and chaotic dynamics that are common for high-power lasers[98]. Complex wave interference effects in these systems disrupt nonlinear processes that form self-organized structures such as filaments, resulting in stable lasing dynamics. In a multimode fiber laser, spatio-temporal mode-locking is achieved[99], paving the way for full control of the spatio-temporal coherence.

The "passive" schemes of manipulating laser performance via cavity geometry and internal structure may be combined with the "active" control with gain and/or loss[100]. Adaptive shaping of the spatial distribution of the pump intensity enables not only single-mode lasing at any selected wavelength[101,102], but also switching of emission directions[103,104]. A symmetric arrangement of gain and loss in a microcavity (Parity-Time symmetry) results in stable single-mode operation[105,106]. Optical loss can induce suppression and revival of lasing in the vicinity of an exceptional point[107,108].

Since a complex laser has numerous degrees of freedom, it may be used for reservoir computing[109]. The self-adaptive nature of a highly multimode laser is exploited for rapid phase retrieval[110]. Imposing constraints in a digital degenerate cavity laser breaks the degeneracy between the transverse modes, and forces the system to find a lasing state with minimal loss. In this manner, the complex lasers can be mapped to hard computational problems and used as physical simulators[111].

To conclude, the study of complex lasers bridges multiple disciplines including mesoscopic physics, nonlinear dynamics, quantum optics, wave-dynamical chaos, and non-Hermitian physics. Thanks to their diversity and versatility, such lasers constitute a toolbox for various applications, allowing application-driven laser design. This article reviews only one particular perspective, however, it hints at the enormous and largely unexplored potential of these systems.

Bibliography

1   Siegman, A. E. *Lasers*. (University Science Books, 1986).

2   Mandel, L. & Wolf, E. *Optical coherence and quantum optics*. (Cambridge university press, 1995).

3   Friberg, A. T. & Setala, T. Electromagnetic theory of optical coherence [Invited]. *J Opt Soc Am A* **33**, 2431-2442, doi:10.1364/Josaa.33.002431 (2016).

4   Chellappan, K. V., Erden, E. & Urey, H. Laser-based displays: a review. *Appl Optics* **49**, F79-F98 (2010).

5   Dainty, J. C. *Laser speckle and related phenomena*. Vol. 9 (Springer science & business Media, 2013).

6   Goodman, J. W. *Speckle phenomena in optics: theory and applications*. (Roberts and Company Publishers, 2007).

7   Lowenthal, S. & Joyeux, D. Speckle Removal by a Slowly Moving Diffuser Associated with a Motionless Diffuser. *J Opt Soc Am* **61**, 847 (1971).

8   Redding, B., Allen, G., Dufresne, E. R. & Cao, H. Low-loss high-speed speckle reduction using a colloidal dispersion. *Appl Optics* **52**, 1168-1172 (2013).

9   Akram, M. N., Tong, Z. M., Ouyang, G. M., Chen, X. Y. & Kartashov, V. Laser speckle reduction due to spatial and angular diversity introduced by fast scanning micromirror. *Appl Optics* **49**, 3297-3304 (2010).

10   Chriki, R. *et al.* Spatio-Temporal Supermodes: Rapid Reduction of Spatial Coherence in Highly Multimode Lasers. *arXiv preprint arXiv:1804.09306, accepted for publication in Phys Rev A* (2018).

11   Cao, H. Lasing in disordered media. *Prog Optics* **45**, 317-370, doi:Doi 10.1016/S0079-6638(03)80008-2 (2003).

12   Noginov, M. A. & Letokhov, V. S. *Solid-state random lasers*. (Springer, 2005).

13   Wiersma, D. S. The physics and applications of random lasers. *Nat Phys* **4**, 359-367, doi:10.1038/nphys971 (2008).

14   Cao, H. *et al.* Random laser action in semiconductor powder. *Phys Rev Lett* **82**, 2278-2281 (1999).

15   Cao, H. *et al.* Ultraviolet lasing in resonators formed by scattering in semiconductor polycrystalline films. *Applied Physics Letters* **73**, 3656-3658 (1998).

16   Lawandy, N. M., Balachandran, R. M., Gomes, A. S. L. & Sauvain, E. Laser Action in Strongly Scattering Media. *Nature* **368**, 436-438 (1994).

17   Frolov, S. V., Vardeny, Z. V., Yoshino, K., Zakhidov, A. & Baughman, R. H. Stimulated emission in high-gain organic media. *Physical Review B* **59**, R5284-R5287 (1999).

18   Turitsyn, S. K. *et al.* Random distributed feedback fibre lasers. *Phys Rep* **542**, 133-193 (2014).

19   Siddique, M., Yang, L., Wang, Q. Z. & Alfano, R. R. Mirrorless Laser Action from Optically Pumped Dye-Treated Animal-Tissues. *Opt Commun* **117**, 475-479 (1995).

20   Leong, E. S. P. & Yu, S. F. UV random lasing action in p-SiC(4H)/i-ZnO-SiO2 nanocomposite/n-ZnO : Al heterojunction diodes. *Adv Mater* **18**, 1685 (2006).

21   Hokr, B. H. *et al.* Bright emission from a random Raman laser. *Nat Commun* **5**, 4356 (2014).

22   Liang, H. K. *et al.* Electrically Pumped Mid-Infrared Random Lasers. *Adv Mater* **25**, 6859-6863 (2013).

23   Schonhuber, S. *et al.* Random lasers for broadband directional emission. *Optica* **3**, 1035-1038 (2016).

24   Vanneste, C., Sebbah, P. & Cao, H. Lasing with resonant feedback in weakly scattering random systems. *Phys Rev Lett* **98**, 143902, doi:10.1103/PhysRevLett.98.1436902 (2007).

25   Redding, B., Choma, M. A. & Cao, H. Spatial coherence of random laser emission. *Opt Lett* **36**, 3404-3406, doi:Doi 10.1364/Ol.36.003404 (2011).

26   Letokhov, V. S. Generation of Light by a Scattering Medium with Negative Resonance Absorption. *Sov Phys Jetp-Ussr* **26**, 835 (1968).

27   Wiersma, D. S. & Lagendijk, A. Light diffusion with gain and random lasers. *Phys Rev E* **54**, 4256-4265 (1996).

28   Jiang, X. Y. & Soukoulis, C. M. Time dependent theory for random lasers. *Phys Rev Lett* **85**, 70-73 (2000).

29   Burin, A. L., Ratner, M. A., Cao, H. & Chang, R. P. H. Model for a random laser. *Phys Rev Lett* **87**, 215503 (2001).

30   Vanneste, C. & Sebbah, P. Selective excitation of localized modes in active random media. *Phys Rev Lett* **87**, 183903 (2001).

31   Ling, Y. *et al.* Investigation of random lasers with resonant feedback. *Phys Rev A* **64**, 063808, doi:10.1103/PhysRevA.64.063808 (2001).

32   Cao, H., Ling, Y., Xu, J. Y. & Burin, A. L. Probing localized states with spectrally resolved speckle techniques. *Phys Rev E* **66**, 025601(R) (2002).

33   El-Dardiry, R. G. S., Mosk, A. P., Muskens, O. L. & Lagendijk, A. Experimental studies on the mode structure of random lasers. *Phys Rev A* **81**, 043830 (2010).

34   Gouedard, C., Husson, D., Sauteret, C., Auzel, F. & Migus, A. Generation of Spatially Incoherent Short Pulses in Laser-Pumped Neodymium Stoichiometric Crystals and Powders. *J Opt Soc Am B* **10**, 2358-2363 (1993).

35   Noginov, M. A., Egarievwe, S. U., Noginova, N., Caulfield, H. J. & Wang, J. C. Interferometric studies of coherence in a powder laser. *Opt Mater* **12**, 127-134, doi:Doi 10.1016/S0925-3467(98)00054-8 (1999).

36   Papadakis, V. M. *et al.* Single-shot temporal coherence measurements of random lasing media. *J Opt Soc Am B* **24**, 31-36 (2007).

37   Cao, H. Review on latest developments in random lasers with coherent feedback. *J Phys a-Math Gen* **38**, 10497-10535, doi:10.1088/0305-4470/38/49/004 (2005).

38   Ambartsumyan, R. V., Kryukov, P. G., Letokhov, V. S. & Matveets, Y. A. Statistical Emission Properties of a Nonresonant Feedback Laser. *Sov Phys Jetp-Ussr* **26**, 1109 (1968).

39   Zacharakis, G., Papadogiannis, N. A., Filippidis, G. & Papazoglou, T. G. Photon statistics of laserlike emission from polymeric scattering gain media. *Opt Lett* **25**, 923-925 (2000).

40   Letokhov, V. S. Quantum Statistics of Multi-Mode Radiation from an Ensemble of Atoms. *Sov Phys Jetp-Ussr* **26**, 1246 (1968).

41   Florescu, L. & John, S. Photon statistics and coherence in light emission from a random laser. *Phys Rev Lett* **93**, 013602 (2004).

42   Beenakker, C. W. J. Photon statistics of a random laser. *Nato Adv Sci I C-Mat* **531**, 137-164 (1999).

43   Cao, H., Ling, Y., Xu, J. Y., Cao, C. Q. & Kumar, P. Photon statistics of random lasers with resonant feedback. *Phys Rev Lett* **86**, 4524-4527 (2001).

44   Garcia-Revilla, S. *et al.* Coherence characteristics of random lasing in a dye doped hybrid powder. *J Lumin* **169**, 472-477 (2016).

45   Cao, H. & Wiersig, J. Dielectric microcavities: Model systems for wave chaos and non-Hermitian physics. *Rev Mod Phys* **87**, 61-111, doi:10.1103/RevModPhys.87.61 (2015).

46   Tureci, H. E., Schwefel, H. G. L., Jacquod, P. & Stone, A. D. Modes of wave-chaotic dielectric resonators. *Progress in Optics* **47**, 75-137 (2005).

47   Stöckmann, H.-J. *Quantum chaos : an introduction*. (Cambridge University Press, 1999).

48   Harayama, T. & Shinohara, S. Two-dimensional microcavity lasers. *Laser Photonics Rev* **5**, 247-271, doi:10.1002/lpor.200900057 (2011).

49   Bunimovich, L. A. Ergodic Properties of Nowhere Dispersing Billiards. *Commun Math Phys* **65**, 295-312 (1979).

50   Redding, B. *et al.* Low spatial coherence electrically pumped semiconductor laser for speckle-free full-field imaging. *P Natl Acad Sci USA* **112**, 1304-1309 (2015).

51   Sale, T. E. *Vertical cavity surface emitting lasers*. (Research Studies Press, Wiley, 1995).

52   Hegarty, S. P., Huyet, G., McInerney, J. G. & Choquette, K. D. Pattern formation in the transverse section of a laser with a large fresnel number. *Phys Rev Lett* **82**, 1434-1437 (1999).

53   Huang, K. F., Chen, Y. F., Lai, H. C. & Lan, Y. P. Observation of the wave function of a quantum billiard from the transverse patterns of vertical cavity surface emitting lasers. *Phys Rev Lett* **89**, 224102 (2002).

54   Gensty, T. *et al.* Wave chaos in real-world vertical-cavity surface-emitting lasers. *Phys Rev Lett* **94**, 233901 (2005).

55   Valle, A., Sarma, J. & Shore, K. A. Dynamics of Transverse-Mode Competition in Vertical-Cavity Surface-Emitting Laser-Diodes. *Opt Commun* **115**, 297-302 (1995).

56   Giudici, M., Tredicce, J. R., Vaschenko, G., Rocca, J. J. & Menoni, C. S. Spatio-temporal dynamics in vertical cavity surface emitting lasers excited by fast electrical pulses. *Opt Commun* **158**, 313-321 (1998).

57   Barchanski, A., Gensty, T., Degen, C., Fischer, I. & Elsäßer, W. Picosecond emission dynamics of vertical-cavity surface-emitting lasers: Spatial, spectral, and polarization-resolved characterization. *Ieee J Quantum Elect* **39**, 850-858 (2003).

58   Peeters, M. *et al.* Spatial decoherence of pulsed broad-area vertical-cavity surface-emitting lasers. *Opt Express* **13**, 9337-9345, doi:Doi 10.1364/Opex.13.009337 (2005).

59   Mandre, S. K., Elsäßer, W., Fischer, I., Peeters, M. & Verschaffelt, G. Evolution from modal to spatially incoherent emission of a broad-area VCSEL. *Opt Express* **16**, 4452-4464, doi:Doi 10.1364/Oe.16.004452 (2008).

60   Craggs, G., Verschaffelt, G., Mandre, S. K., Thienpont, H. & Fischer, I. Thermally Controlled Onset of Spatially Incoherent Emission in a Broad-Area Vertical-Cavity Surface-Emitting Laser. *Ieee J Sel Top Quant* **15**, 555-562, doi:10.1109/Jstqe.2009.2016355 (2009).

61   Riechert, F. *et al.* Speckle characteristics of a broad-area VCSEL in the incoherent emission regime. *Opt Commun* **281**, 4424-4431, doi:10.1016/j.optcom.2008.05.004 (2008).

62   Michalzik, R. *VCSELs : fundamentals, technology and applications of vertical-cavity surface-emitting lasers*. (Springer, 2013).

63   Knitter, S. *et al.* Coherence switching of a degenerate VECSEL for multimodality imaging. *Optica* **3**, 403-406, doi:10.1364/Optica.3.000403 (2016).

64   Arnaud, J. A. Degenerate optical cavities. *Appl Optics* **8**, 189-196 (1969).

65   Pole, R. Conjugate-concentric laser resonator. *JOSA* **55**, 254-260 (1965).

66   Nixon, M., Redding, B., Friesem, A. A., Cao, H. & Davidson, N. Efficient method for controlling the spatial coherence of a laser. *Opt Lett* **38**, 3858-3861, doi:10.1364/Ol.38.003858 (2013).

67   Chriki, R. *et al.* Manipulating the spatial coherence of a laser source. *Opt Express* **23**, 12989-12997, doi:10.1364/Oe.23.012989 (2015).

68   Desurvire, E. *Erbium-doped fiber amplifiers : principles and applications*. (Wiley-Interscience, 2002).

69   Zervas, M. N. & Codemard, C. A. High Power Fiber Lasers: A Review. *Ieee J Sel Top Quant* **20**, 0904123 (2014).

70   Cheng, M.-Y. *et al.* High-energy and high-peak-power nanosecond pulse generation with beam quality control in 200-µm core highly multimode Yb-doped fiber amplifiers. *Opt Lett* **30**, 358-360 (2005).

71   Florentin, R. *et al.* Shaping the light amplified in a multimode fiber. *Light: Science & Applications* **6**, e16208 (2017).

72   Florentin, R., Kermene, V., Desfarges-Berthelemot, A. & Barthelemy, A. Space-time adaptive control of femtosecond pulses amplified in a multimode fiber. *Opt Express* **26**, 10682-10690 (2018).

73   Redding, B. *et al.* Low-spatial-coherence high-radiance broadband fiber source for speckle free imaging. *Opt Lett* **40**, 4607-4610, doi:10.1364/Ol.40.004607 (2015).

74   Hartmann, S. & Elsäßer, W. A novel semiconductor-based, fully incoherent amplified spontaneous emission light source for ghost imaging. *Sci Rep-Uk* **7** (2017).

75   Goodman, J. W. Statistical optics. (2015).

76   Glenzer, S. H. *et al.* Progress in long scale length laser-plasma interactions. *Nucl Fusion* **44**, S185-S190, doi:10.1088/0029-5515/44/12/S08 (2004).

77   Dhalla, A. H., Migacz, J. V. & Izatt, J. A. Crosstalk rejection in parallel optical coherence tomography using spatially incoherent illumination with partially coherent sources. *Opt Lett* **35**, 2305-2307, doi:Doi 10.1364/Ol.35.002305 (2010).

78   Papagiakoumou, E. *et al.* Functional patterned multiphoton excitation deep inside scattering tissue. *Nat Photonics* **7**, 274-278, doi:10.1038/Nphoton.2013.9 (2013).

79   Redding, B., Choma, M. A. & Cao, H. Speckle-free laser imaging using random laser illumination. *Nat Photonics* **6**, 355-359, doi:10.1038/Nphoton.2012.90 (2012).

80   Hokr, B. H. *et al.* A narrow-band speckle-free light source via random Raman lasing. *J Mod Optic* **63**, 46-49, doi:10.1080/09500340.2015.1078919 (2016).

81   Haeusler, G. in *Encyclopedia of Modern Optics* Vol. 1   114-123 (Elsevier Ltd., 2004).

82   Mermillod-Blondin, A., Mentzel, H. & Rosenfeld, A. Time-resolved microscopy with random lasers. *Opt Lett* **38**, 4112-4115 (2013).

83   Webb, R. H. Confocal optical microscopy. *Rep Prog Phys* **59**, 427-471 (1996).

84   Corle, T. R. & Kino, G. S. *Confocal scanning optical microscopy and related imaging systems*. (Academic Press, 1996).

85   Petran, M., Hadravsky, M., Egger, M. D. & Galambos, R. Tandem-Scanning Reflected-Light Microscope. *J Opt Soc Am* **58**, 661 (1968).

86   Somekh, M. G., See, C. W. & Goh, J. Wide field amplitude and phase confocal microscope with speckle illumination. *Opt Commun* **174**, 75-80 (2000).

87   Redding, B., Bromberg, Y., Choma, M. A. & Cao, H. Full-field interferometric confocal microscopy using a VCSEL array. *Opt Lett* **39**, 4446-4449, doi:10.1364/Ol.39.004446 (2014).

88   Liu, C. G., Cao, H. & Choma, M. A. Coherent artifact suppression in line-field reflection confocal microscopy using a low spatial coherence light source. *Opt Lett* **41**, 4775-4778, doi:10.1364/Ol.41.004775 (2016).

89   Sencan, I. *et al.* Ultrahigh-speed, phase-sensitive full-field interferometric confocal microscopy for quantitative microscale physiology. *Biomed Opt Express* **7**, 4674-4684, doi:10.1364/Boe.7.004674 (2016).

90   Boas, D. A. & Dunn, A. K. Laser speckle contrast imaging in biomedical optics. *J Biomed Opt* **15**, 011109 (2010).

91   Munro, E. A., Levy, H., Ringuette, D., O'Sullivan, T. D. & Levi, O. Multi-modality optical neural imaging using coherence control of VCSELs. *Opt Express* **19**, 10747-10761, doi:10.1364/Oe.19.010747 (2011).

92   Dickey, F. M. & Holswade, S. C. *Laser beam shaping : theory and techniques*. (Marcel Dekker, 2000).

93   Liew, S. F. *et al.* Intracavity frequency-doubled degenerate laser. *Opt Lett* **42**, 411-414 (2017).

94   Turunen, J., Vasara, A. & Friberg, A. T. Propagation Invariance and Self-Imaging in Variable-Coherence Optics. *J Opt Soc Am A* **8**, 282-289, doi:Doi 10.1364/Josaa.8.000282 (1991).

95   Chriki, R. *et al.* Rapid and efficient formation of propagation invariant shaped laser beams. *Opt Express* **26**, 4431-4439, doi:10.1364/OE.26.004431 (2018).

96   Nixon, M. *et al.* Real-time wavefront shaping through scattering media by all-optical feedback. *Nat Photonics* **7**, 919-924, doi:10.1038/Nphoton.2013.248 (2013).

97   Chriki, R. *et al.* Spin-controlled twisted laser beams: intra-cavity multi-tasking geometric phase metasurfaces. *Opt Express* **26**, 905-916 (2018).

98   Bittner, S. *et al.* Taming spatio-temporal lasing instabilities with wave-chaotic microcavities. *Arxiv preprint arXiv:1802.02028v1* (2018).

99   Wright, L. G., Christodoulides, D. N. & Wise, F. W. Spatiotemporal mode-locking in multimode fiber lasers. *Science* **358**, 94-97 (2017).

100   Andreasen, J. *et al.* Partially Pumped Random Lasers. *Int J Mod Phys B* **28**, doi:10.1142/S0217979214300011 (2014).

101   Bachelard, N., Gigan, S., Noblin, X. & Sebbah, P. Adaptive pumping for spectral control of random lasers. *Nat Phys* **10**, 426-431, doi:10.1038/Nphys2939 (2014).

102   Liew, S. F., Ge, L., Redding, B., Solomon, G. S. & Cao, H. Pump-controlled modal interactions in microdisk lasers. *Phys Rev A* **91**, doi:10.1103/PhysRevA.91.043828 (2015).

103   Liew, S. F., Redding, B., Ge, L., Solomon, G. S. & Cao, H. Active control of emission directionality of semiconductor microdisk lasers. *Applied Physics Letters* **104**, doi:10.1063/1.4883637 (2014).

104   Hisch, T., Liertzer, M., Pogany, D., Mintert, F. & Rotter, S. Pump-Controlled Directional Light Emission from Random Lasers. *Phys Rev Lett* **111**, doi:10.1103/PhysRevLett.111.023902 (2013).

105   Feng, L., Wong, Z. J., Ma, R. M., Wang, Y. & Zhang, X. Single-mode laser by parity-time symmetry breaking. *Science* **346**, 972-975, doi:10.1126/science.1258479 (2014).

106   Hodaei, H., Miri, M. A., Heinrich, M., Christodoulides, D. N. & Khajavikhan, M. Parity-time-symmetric microring lasers. *Science* **346**, 975-978, doi:10.1126/science.1258480 (2014).

107   Liertzer, M. *et al.* Pump-Induced Exceptional Points in Lasers. *Phys Rev Lett* **108**, doi:10.1103/PhysRevLett.108.173901 (2012).

108   Peng, B. *et al.* Loss-induced suppression and revival of lasing. *Science* **346**, 328-332, doi:10.1126/science.1258004 (2014).

109   Brunner, D., Soriano, M. C., Mirasso, C. R. & Fischer, I. Parallel photonic information processing at gigabyte per second data rates using transient states. *Nat Commun* **4**, doi:10.1038/ncomms2368 (2013).

110   Tradonsky, C. *et al.* Rapid Phase Retrieval by Lasing. *arXiv preprint arXiv:1805.10967* (2018).

111   McMahon, P. L. *et al.* A fully programmable 100-spin coherent Ising machine with all-to-all connections. *Science* **354**, 614-617, doi:10.1126/science.aah5178 (2016).